Growth and rapid succession of methanotrophs effectively limit methane release during lake overturn

*Magdalena J. Mayr[1,2], Matthias Zimmermann[1,2], Jason Dey[1], Andreas Brand[1,2], Helmut Bürgmann[1]

[1]Department of Surface Waters—Research and Management, Eawag, Swiss Federal Institute of Aquatic Science and Technology, Kastanienbaum, Switzerland

[2]Institute of Biogeochemistry and Pollutant Dynamics, Department of Environmental Systems Science, ETH Zurich, Swiss Federal Institute of Technology, Zurich, Switzerland

*Corresponding author: Magdalena J. Mayr, Seestrasse 79, 6047 Kastanienbaum, +41 58 765 2142, magdalena.mayr@eawag.ch

Abstract

Lakes and reservoirs contribute substantially to atmospheric concentrations of the potent greenhouse gas methane. Lacustrine sediments produce large amounts of methane, which accumulate in oxygen-depleted hypolimnia of stratified lakes. Due to climate change and progressing eutrophication, the number of lakes with hypolimnetic methane storage may increase in the future. However, whether stored methane eventually reaches the atmosphere during lake overturn is a matter of controversy and depends critically on the response of the methanotroph assemblage. We show that the methanotroph assemblage in a mixing lake undergoes a substantial bloom and ecological succession. As a result, the methane oxidation capacity of the mixed layer kept pace with the methane supplied from the hypolimnion and most of the stored methane was oxidized. Our work demonstrates a previously unknown component of freshwater methanotroph ecology illuminating the mechanisms limiting methane transfer from lakes to the atmosphere.

Introduction

Lakes and impoundments emit a GHG equivalent of 20% of the global fossil fuel CO_2 emissions, with methane contributing 75% of these CO_2 equivalents (DelSontro et al. 2018). Stratified lakes accumulate the strong greenhouse gas methane in their oxygen-depleted bottom waters (Bastviken et al. 2002). During lake overturn this methane may reach the surface layer, thereby running the risk of outgassing. Despite the established importance of lakes for global GHG emissions, the fate of methane during the overturn period is currently understudied (DelSontro et al. 2018). Two competing hypotheses regarding the fate of methane in this period have been discussed. According to the first all or most of the stored methane will be released into the atmosphere (Bastviken et al. 2004). If this hypothesis is correct, the stored methane would need to be added to lake methane emission estimates. According to the second hypothesis, methanotrophs oxidize most of the methane with oxygen to CO_2, which has a 34 times lower global warming potential for a 100-yr time-scale (Myhre et al. 2013) and sequester a small proportion as biomass. Some previous estimates assumed overturn to occur on very short time scales, e.g. a single day (Bastviken et al. 2004) therefore favoring the first hypothesis. Other studies have indicated that lake overturn typically takes place on a scale of weeks to months, even in shallow lakes (Kankaala et al. 2007, Taipale et al. 2011, Schubert et al. 2012), which may allow time for significant methane oxidation. This controversy has not yet been resolved (Encinas Fernández et al. 2014) and the importance of methane-oxidizing bacteria (MOB) during lake overturn remains to be explored.

MOB in lakes have mostly been investigated during the stratified season, when a structured MOB assemblage forms an efficient methane filter preventing the methane accumulating in the bottom water from outgassing (Kojima et al. 2009, Biderre-Petit et al. 2011, Blees et al. 2014, Oswald et al. 2017). How the MOB assemblage responds to lake overturn remains unknown, but its growth rate and resulting methane oxidation capacity is critical for the amount of methane emitted. During lake overturn environmental conditions change compared to the stratified lake (Salcher 2014). The lake

47 cools down and oxygen and methane, which are vertically separated during stratification, become
48 available simultaneously as water layers with different substrate and nutrient concentrations mix.

49 Here we present a field study over the entire three months of the autumn lake overturn of shallow
50 eutrophic Lake Rotsee, Switzerland. We asked (i) if the MOB assemblage grows fast enough to oxidize
51 the methane mobilized from the bottom water before outgassing and (ii) if the standing MOB
52 assemblage is activated, or a new assemblage successively takes over in the changing lake. We used
53 16S rRNA gene amplicon sequencing, *pmoA* mRNA sequencing and qPCR, potential methane oxidation
54 rates and CARD-FISH to investigate succession, growth and methane oxidation capacity of the MOB
55 assemblage during lake overturn. The study provides an unprecedented insight into the dynamics of
56 freshwater lake MOB and shows that a new and highly abundant MOB assemblage, representing up
57 to 28% of 16S rRNA gene sequences, thrived in the expanding mixed layer. Along with the MOB
58 assemblage, the methane oxidation capacity of the lake increased substantially, thereby limiting the
59 emitted methane to a small percentage of the stored methane. The rates of physical mixing and the
60 transfer and transformation of methane have been analyzed with a process-based model in a parallel
61 study (Zimmermann et al. 2019).

Results

Characteristics of stratification and overturn dynamics

To determine the response of the MOB assemblage and methane oxidation activity to lake overturn, we sampled the shallow eutrophic Lake Rotsee at eight time points covering stratification, overturn and inverse stratification. The starting point of our sampling campaign on October 04 represents a typical stratified situation which starts to develop in Rotsee in May (Schubert et al. 2010). Until Oct 04 large amounts of methane have accumulated in the hypolimnion, which we refer to as 'stored methane' in the following.

Most of oxygen and the stored methane are separated from each other prior to lake overturn (Fig. 1A). The lake cooled down from October to January, resulting in a gradual expansion of the mixed layer until December (Fig. 1B). By Dec 12th a cooler mixed layer was on top of warmer bottom water (Fig. 1B), caused by slightly increased salinity of the warmer bottom water (Supplementary Fig. 1). From October to December, a total of 4.2 Mg C of stored methane gradually entered the mixed layer (Zimmermann et al. 2019). But nevertheless median methane concentrations stayed low in mixed layer ranging from 0.1 – 1.1 µM. Oxygen levels in the mixed layer dropped down to approx. 175 µM

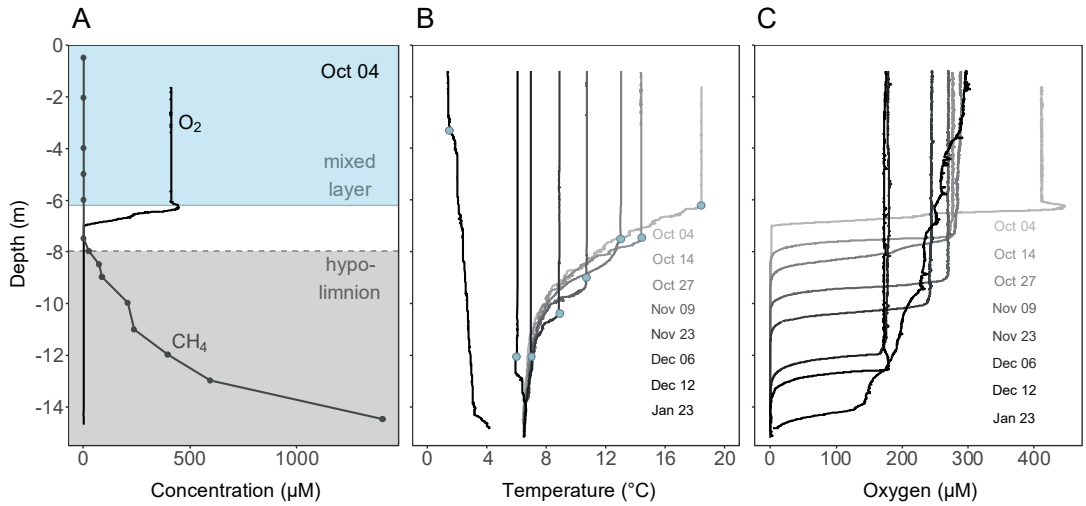

Figure 1 A) Stratified situation in Rotsee prior to lake overturn. Oxygen in the mixed layer and methane in the hypolimnion are separated from each other prior to lake overturn. The methane-enriched hypolimnion (≥ 2 µM) is shaded in gray, the mixed layer is shaded in blue. **B)** Temperature profiles of the cooling lake in autumn and winter and the resulting expansion of the mixed layer. Blue dots indicate the mixed layer depth. In January an inverse stratification established. **C)** Corresponding oxygen profiles at each sampling date.

77 (Dec 12, Fig. 1C), likely due to methane and other reduced substances from the hypolimnion triggering
78 abiotic and biotic oxygen consumption. From December to January, oxygen concentrations increased
79 again.

80 The methane oxidizing assemblage prior to lake overturn

81 We analyzed the MOB assemblage with a set of independent and mutually supportive methods. We
82 used 16S rRNA gene sequencing to phylogenetically identify known groups of MOB, to estimate their
83 proportion of the bacterial community and to assess MOB assemblage dynamics. The *pmoA* mRNA
84 sequencing combined with qPCR provided an independent assessment of the MOB assemblage as well
85 as confirmation of transcriptional activity of the methane monooxygenase. To facilitate interpretation,
86 we assigned the same colors for MOB ASVs (MOB-affiliated 16S rRNA amplicon sequence variants)
87 and aaASVs (*pmoA* amino acid operational taxonomic units), if they showed similar relative abundance
88 and distribution pattern in a canonical correspondence analysis (Supplementary Fig. 2) and
89 compatibility with the phylogenetic tree (Supplementary Fig. 3).

90 On October 04, the proportion of MOB ASVs and the copy number of *pmoA* transcripts peaked at the
91 upper boundary of the methane-enriched hypolimnion, although both measures showed that MOB
92 were present throughout the water column (Oct 04, Fig. 2A, B). The hypolimnion harbored a higher
93 proportion of MOB ASVs and *pmoA* transcripts than the oxygen-rich mixed layer. Therefore, it
94 represents a potential reservoir of MOB for the following lake overturn. The composition of the MOB
95 assemblage differed strongly between the mixed layer and hypolimnion. The mixed layer was
96 dominated by gammaproteobacterial type Ia MOB (Fig. 2A, B, blue) assigned to uncultivated groups
97 CABC2E06/Lake cluster1 (ASV_5/aaASV1 and aaASV6). According to 16S rRNA gene-based analysis a
98 *Methylocystis* (ASV_354, yellow) was also dominant, however the corresponding aaASV7 *pmoA*
99 transcript was rather underrepresented in the assemblage (Supplementary Fig. 4). In the hypolimnion
100 other uncultivated type I MOB closely related to lacustrine Crenothrix prevailed (ASV_8, 35, 81, 95.6-
101 96.7% identity and aaASV2, 3, 8, 96.1-97.4% identity to lacustrine Crenothrix; shown in shades of pink,

Fig. 2A, B). In between the mixed layer and the methane-enriched hypolimnion the abundance of additional MOB sequences peaked, e.g. ASV_166 (Supplementary Fig. 4A) and aaASV12.

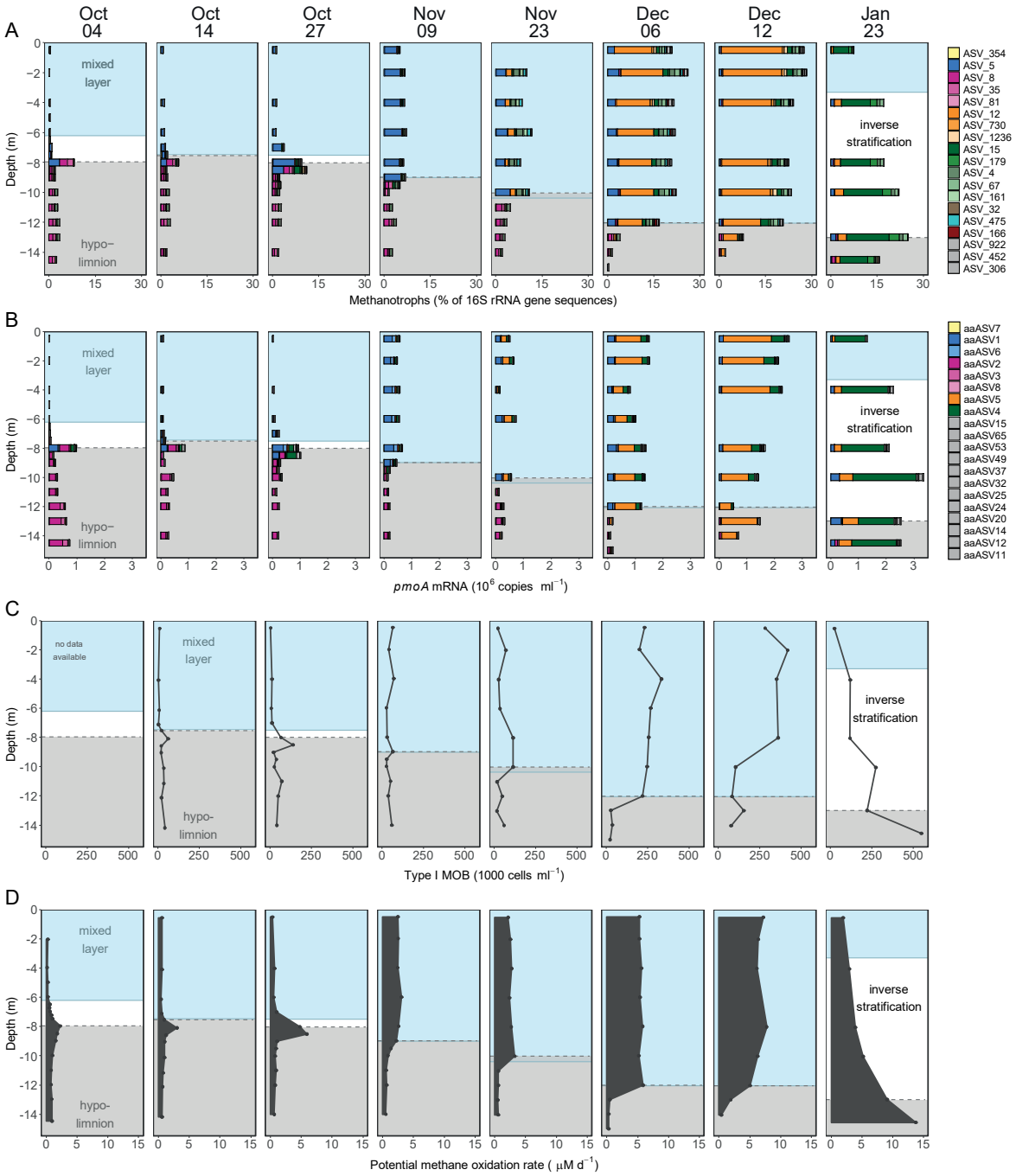

Figure 2 Depth distribution and dynamics of the MOB assemblage, *pmoA* transcripts, MOB cell numbers and potential methane oxidation rates during lake overturn. The mixed layer (blue background) depth increased with time, while the methane-rich hypolimnion (≥ 2 µM, gray background) got gradually incorporated into the mixed layer. **A)** MOB are shown as a proportion of all bacterial 16S rRNA gene sequences and colors distinguish MOB at the ASV level. **B)** A similar pattern is seen in *pmoA* transcript abundance derived from qPCR quantification (copies ml^{-1}) multiplied with the relative abundance of *pmoA* mRNA aaASVs from sequencing. Colors correspond to aaASVs. ASVs and aaASVs which, based on multiple lines of evidence (see methods), are thought to originate from the same organism are encoded with the same color. **C)** MOB cell abundance (1000 cells ml^{-1}) as determined by CARD-FISH and **D)** potential methane oxidation rates in µM day^{-1} measured in incubations with $^{13}C\text{-}CH_4$.

MOB dynamics at the onset of the overturn

By Oct 27 we observed an increase of MOB abundance and *pmoA* transcripts at the upper boundary of the methane-enriched hypolimnion (Fig. 2A, B). Although the mixed layer depth increased throughout October it did not yet reach the methane-enriched hypolimnion (Fig. 2A, B). However, the deepening of the mixed layer brought the oxygen-rich mixed layer closer to the methane-enriched hypolimnion, likely increasing the downward oxygen flux.

By November 09 the mixed layer had finally reached and eroded a small part of the methane-enriched hypolimnion (Fig. 2A, B). The MOB observed in the peak from Oct 27 had thus likely been entrained into the mixed layer. It is likely that both CABC2E06 (ASV_5/aaASV1 and 6, blue), as well as Crenothrix-related MOB (ASV_8/aaASV2, pink) were transported into the mixed layer. However, only the members of the CABC2E06 group (blue), which already prevailed in the mixed layer in Oct showed up in as the dominant MOB in the mixed layer (Fig. 2A, B, Supplementary Fig. 4). Thus, both transport of MOB to and their growth in the mixed layer may have contributed to the increased MOB percentage and *pmoA* transcripts observed on Nov 09 (Fig. 2A, B). From Nov 09 onwards, we no longer observed the MOB peak formation typical for the stratified period at the oxygen-methane interface, likely because the interface was constantly moving downwards as the mixed layer deepened (Fig. 2A, B).

Dynamics of the MOB assemblage during overturn

From Nov 09 to Dec 12 the mixed layer deepened from 9 m to 12 m, thereby incorporating large amounts of stored methane. It must be assumed that the MOB assemblage from the hypolimnion was continuously transported into the mixed layer. However, the Crenothrix-related MOB that dominated there (Fig. 2A, B) were only detected at very low abundances in the mixed layer. Instead, a MOB with 97.2% sequence identity to *Methylosoma difficile* (ASV_12/aaASV5, Supplementary Fig. 3A) rapidly increased, peaking at a median percentage of 16% of all bacterial sequences in the mixed layer on Dec 12 (Fig. 2A, B, orange). All MOB sequences together reached up to 28% of the bacterial sequences on

128 Dec 12, with ASV_12 as the most important contributor to the increase in MOB abundance. ASV_12
129 was already present in October, but at very low proportion with a maximum of 0.2% of the bacterial
130 sequences.

131 In January, an inverse stratification formed and only close to the bottom of the lake (16 m max. depth)
132 a small part of the water column with stored methane remained. MOB proportion and mRNA copy
133 numbers of ASV_12/aaASV5 decreased and the MOB assemblage shifted again with ASV_15/aaASV4
134 (green, Fig. 2A, B) now dominating the MOB assemblage.

135 Dynamics of potential methane oxidation capacity and MOB cell numbers

136 In October, type I MOB cell numbers as determined by CARD-FISH peaked at the upper boundary of
137 the methane-enriched hypolimnion, corroborating the patterns observed from MOB ASVs and *pmoA*
138 mRNA transcripts. Further, potential methane oxidation rates showed a strikingly similar pattern,
139 suggesting that the MOB assemblages present were active. Even within the oxygen-depleted
140 hypolimnion, potential methane oxidation rates never fell below 0.3 µM d^{-1} (Fig. 2C). Throughout the
141 lake overturn MOB cell numbers and potential methane oxidation rates increased substantially within
142 the mixed layer (Fig. 2C, D). Not only had the potential methane oxidation rates reached and, by Dec
143 12, exceeded the maximum rates usually found only in a narrow layer at the oxygen-methane interface
144 during stable stratification, but the water volume with these high rates had also increased (Fig. 2D). In
145 combination, this led to an overall increase of the potential methane oxidation capacity from 0.01 Mg
146 C d^{-1} on Oct 04 up to 0.3 Mg C d^{-1} within the mixed layer volume on Dec 06 and 12 (Fig. 2D). MOB cell
147 numbers in the mixed layer increased with a net doubling time of approx. 9 days (Oct – Dec 12). The
148 methane oxidation capacity increased as well, although at a slower rate (doubling every 12.7 days in
149 the period of Oct – Dec 12). After lake overturn was complete, i.e. between Dec 12 and Jan 23,
150 potential methane oxidation rates and MOB cell numbers generally decreased at the water depths
151 formerly occupied by the mixed layer. The methane oxidation rates and MOB abundance now

increased with depth and peaked in the remaining methane-enriched bottom layer near the sediment (Fig. 2C, D). All measured MOB parameters were significantly correlated (Supplementary Tab. 1).

Winners and losers: thriving mixed layer MOB and fate of hypolimnetic MOB

The winners of the lake overturn were taxa of the mixed layer MOB assemblage (Fig. 3A), which contributed substantially to the increase of potential methane oxidation rates (Fig. 3B). The profound shift in the composition of the MOB assemblage suggested that the changing physical and chemical conditions in the lake influenced the succession (Fig. 3 and Supplementary Fig. 2).

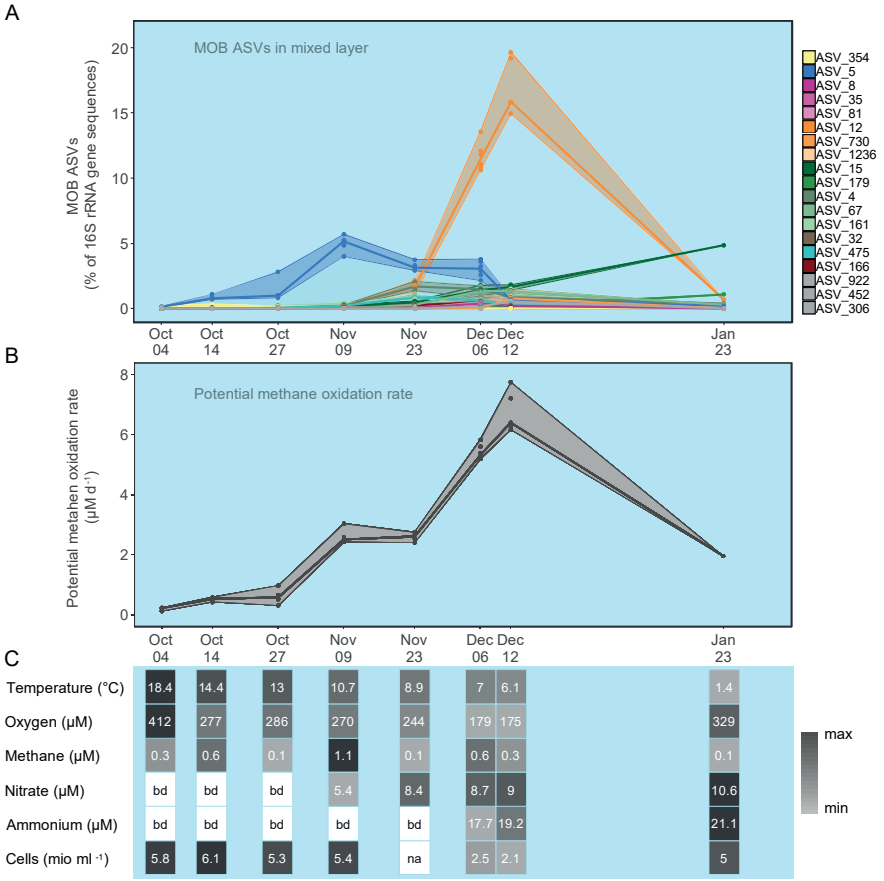

Figure 3 Mixed layer dynamics during lake overturn. **A)** MOB assemblage dynamics at the ASV level within the expanding mixed layer during lake overturn. Maximum, minimum and median relative abundance of each MOB ASV within the mixed layer are visualized with lines. Colors correspond to MOB ASVs. **B)** Dynamics of potential methane oxidation rates during lake overturn. Lines depict maximum, minimum and median within the mixed layer. **C)** Table illustrating the corresponding change in physical, chemical and biological environmental parameters in the mixed layer over time. The median of the mixed layer samples is shown for each parameter and sampling date. Shades of gray are scaled between minimum (light grey) and maximum (black) values. Values below the limit of quantification are marked with "bd" and missing data with "na".

159 The dominance of CABC2E06 (ASV_5) in the oxygen-rich mixed layer until November supports
160 previous observations of this taxon occurring under, and being correlated with, elevated oxygen
161 concentrations during stable stratification in four Swiss lakes (Mayr et al. *in prep*). Our observations in
162 this study further support the view that this MOB taxon thrives under high oxygen concentration and
163 continuous but low concentration methane supply. Despite its occurrence in several lakes and its
164 sometimes high abundance and pivotal role during overturn, lack of a cultured representatives or
165 genomes currently precludes further insights into the ecology of this taxon.

166 The early dominance of CABC2E06 (ASV_5) was followed by a rapid increase of the *Methylosoma*-
167 related ASV_12 until Dec 12, which lead to dominance of this taxon during the lake overturn (orange,
168 Fig. 3A). The growth phase of ASV_12 was accompanied by a drop in water temperature to below 10
169 °C, and increasing nutrient levels in the mixed layer (Fig. 3C). The only cultured representative of
170 *Methylosoma, M. difficile* is microaerophilic (Rahalkar et al. 2007), which is in line with the observation
171 that ASV_12 dominated during the period with the lowest measured oxygen concentration in the
172 mixed layer (175 µM). This taxon was not observed in three other Swiss lakes in a previous study (Mayr
173 et al. in *prep*), and was only detected at very low abundance in the October samples of Rotsee in this
174 campaign. This MOB taxon thus appears to be seasonally restricted or conditionally rare, but
175 nevertheless was the most spectacular profiteer of the lake turnover and highly relevant to methane
176 mitigation during our study period.

177 ASV_15, related to *Methylobacter tundripaludum* (98.6% identity) steadily increased during the later
178 phase of the overturn and dominated the MOB assemblage on Jan 23. At the same time lake water
179 cooled below 4°C, oxygen levels replenished while elevated nutrient levels persisted (Fig. 3C). This
180 finding could perhaps be explained by an adaptation to low temperatures. Previous observations of
181 psychrophily within the *Methylobacter* genus (Trotsenko and Khmelenina 2005) provide some support
182 for this hypothesis.

183 The losers of the lake overturn, Crenothrix-related ASVs/aaASVs (ASV_8, 35, 81 pink), remained
184 restricted to the eroding hypolimnion, until only a tiny fraction was left on Jan 23 (Fig. 2A, B,
185 Supplementary Fig. 4). These were never able to establish in the mixed layer, although these taxa were
186 presumably inoculated continuously into the mixed layer. This suggests that their ecological
187 specialization may be responsible, as proposed earlier (Mayr et al. in *prep*). These MOB taxa resided
188 in water layers with high methane concentrations and are thought to rely on oxygen released from
189 phytoplankton (Oswald et al. 2015) or from temporally and spatially limited nano- to micromolar
190 oxygen intrusions (Kirf et al. 2015). On the other hand, the *Methylobacter tundripaludum*-like ASV_4
191 (99.3% identity) which was present at low abundance in the hypolimnion, gained momentum
192 temporarily in the mixed layer in Nov and Dec (Fig. 3A) suggesting a flexible ecology of this organism.

193 ## Discussion

194 In our study, we provide the first comprehensive analysis of the response of a MOB assemblage to
195 autumn lake overturn. We asked if the MOB assemblage grows fast enough to oxidize the stored
196 methane before outgassing. We revealed that the MOB assemblage is fast enough to counteract
197 methane outgassing during a gradual lake overturn. MOB growth lead to a substantial increase in MOB
198 abundance until MOB made up 28% of the bacterial 16S rRNA gene sequences in the mixed layer (Fig.
199 2). This established a high methane oxidation capacity in the mixed layer. We further asked if the
200 standing MOB assemblage is activated, or a new assemblage successively takes over and found that a
201 temporal succession of MOB taxa built the basis for the increasing MOB abundance and methane
202 oxidation capacity (Fig. 3A, B). Growth of a new MOB assemblage and its methane oxidation capacity
203 limited the emitted methane to a small percentage of the stored methane during lake overturn.

204 There is some evidence that the succession patterns of MOB, similar to vertical niche preferences
205 discussed previously (Mayr et al. *in prep*) are related to specific adaptations of the successful taxa.
206 During the phase with the highest methane oxidation capacity in the lake, the initial MOB assemblage
207 of both mixed layer and methane-enriched hypolimnion had been almost entirely replaced by a new
208 MOB assemblage (Fig. 2). Different MOB reached a high degree of dominance in the MOB assemblage
209 at different stages of the lake overturn. This indicates that the changing environmental conditions
210 during lake overturn favored temporal niche partitioning of MOB taxa (Fig. 3). It is notable, however,
211 that despite the well-mixed situation and the often observed dominance of a single taxon a diverse
212 MOB assemblage was nevertheless present throughout the overturn period. Answering the question
213 if the same or similar MOB are dominating the fall overturn every year will require a longer-term
214 monitoring effort. Presence of MOB taxa with specific adaptation that allow them to take advantage
215 of the rapidly changing conditions in the overturning lake is likely essential to establishing the methane
216 oxidation capacity that ultimately limits methane outgassing.

217 Although methane becomes available in the mixed layer, dilution and rapid oxidation keep
218 concentrations low as opposed to the situation in the hypolimnion (Fig. 3C). MOB in the mixed layer
219 thus likely require a relatively high methane-affinity for growth. We therefore speculate that the
220 methane affinity of the mixed-layer MOB assemblage may be a critical factor for the amount of
221 methane outgassing to the atmosphere. In addition to the inherent methane-affinity of MOB taxa and
222 assemblages, other traits like growth rates and ability to access nutrients likely affect the build-up of
223 the methane-oxidation capacity in the lake and require further exploration.

224 Although the net doubling time of MOB in the expanding mixed layer was 9 days, suggesting slow
225 growth, MOB were able to substantially increase their abundance leading to a total methane oxidation
226 capacity of the mixed layer volume of approximately 0.3 Mg carbon per day (Dec 12). The oxidation
227 capacity estimate is conservative as only potential methane oxidation to CO_2 was measured and
228 incorporation into biomass is not included. Even though the growth rates seem low compared to
229 observations in MOB isolates (Wise et al. 2001) they may be in line with the environmental conditions:
230 temperatures in the mixed layer dropped from 18.4 (Oct 04) to 6.1°C (Dec 12), likely slowing down
231 process and growth rates as the overturn progressed. Further, persistent low methane concentrations
232 despite continuous supply likely reduced effective growth rates. Because of the evident MOB
233 assemblage succession, the doubling time given above represents a sum over all taxa and growth rates
234 of e.g. taxa becoming dominant were certainly faster as other taxa stagnated or decreased in
235 abundance at the same time. Gross growth rates are likely higher as mortality rates are unknown.

236 While some estimates of global methane emissions from lakes assume that all stored methane is
237 emitted to the atmosphere (Bastviken et al. 2004, 2008), our data is in line with other field studies
238 that suggest a considerable proportion of stored methane is oxidized. One study estimated that 46%
239 of the stored methane is emitted during autumn lake overturn (Encinas Fernández et al. 2014), but
240 most estimates are higher, claiming oxidation of 75 – 94% of the stored methane (Utsumi et al. 1998,
241 Kankaala et al. 2007, Schubert et al. 2012). Rotsee methane emission data from eddy-covariance flux

measurements and modelling (Zimmermann et al. 2019) obtained in parallel with this study showed that about 98% of the stored methane was oxidized. Most lakes in temperate regions are holomictic and have a mean lake depth of < 25 m. Worldwide, small (size classes 0.1-1 and 1-10 km^2), relatively shallow (average depth 5 and 5.4 m, respectively) lakes represent 28% of the estimated global lake area (Messager et al. 2016). Methane storage is frequently observed especially in small lakes (Bastviken et al. 2004). Thus, processes as observed in Rotsee may occur in a considerable proportion of temperate lakes and might be important to global methane flux estimates. The precise impact can currently not be estimated and more data from different lake types is needed for reliable extrapolations. Nevertheless, we must caution against adding methane storage to lake emission estimates. Lakes remain significant sources of atmospheric methane: ebullition bypasses biological oxidation and rapid overturn events due to e.g. fast lake cooling and strong winds will lead to increased outgassing (Kankaala et al. 2007, Zimmermann et al. 2019). Nevertheless, the body of evidence on methane emission and oxidation measurements during fall overturn indicates that efficient oxidation of methane during overturn is not an exceptional occurrence, and thus MOB blooms during lake turnover may occur regularly, representing an important aspect of freshwater MOB ecology.

In this comprehensive study we show why most of the stored methane in the hypolimnion is not released to the atmosphere upon autumnal overturn in a eutrophic stratified lake. High MOB abundance enabled by successional changes in the MOB assemblage provided an extraordinarily high methane-oxidation capacity during the lake overturn, thereby greatly reducing the emission of hypolimnetic stored methane from the lake. The successive key players included an uncultivated but common type I MOB taxon associated with the CABC2E06 clade and a conditionally rare MOB taxon of the genus *Methylosoma*. The number of lakes with hypolimnetic methane storage may increase in future due to lack of recovery of lakes from eutrophication (Jenny et al. 2016) and continuing eutrophication of lakes (Beaulieu et al. 2019), while climate change will alter boundary conditions. A comprehensive knowledge on the fate of stored methane in transitionally stratified lakes and

267 information on the adaptability of MOB to different environmental conditions and their methane
268 oxidation kinetics are therefore critical.

269 Methods

270 Environmental sampling and profiling during autumn overturn

271 A temperate holomictic lake, Rotsee (47.072 N and 8.319 E) in Central Switzerland was sampled on 8
272 dates from October 4, 2016 to January 23, 2017. This sampling period covered the end of stratification
273 with maximal methane accumulation in the hypolimnion and the subsequent autumn overturn. A
274 moored thermistor chain (1 m resolution) provided temperature measurements every three hours,
275 documenting the mixing process and serving as a basis for scheduling the sampling dates. At each
276 sampling date continuous profiles of temperature and oxygen (PSt1, Presens, Regensburg, Germany),
277 were measured with the profiling *in-situ* analyzer (PIA) as described previously (Kirf et al. 2014).
278 Sampling depths for further analyses were set based on the PIA profiles. The PIA was equipped with a
279 syringe sampler allowing targeted depth sampling at a high resolution down to 25 cm integrating
280 about 5 cm water column compared to conventional Niskin bottles (>50 cm). The mixed layer depth
281 was defined as the part of the water column with a uniform temperature profile.

282 Water samples for analysis of ammonium, nitrate and dissolved inorganic carbon (DIC) were filtered
283 with a 0.2 µm pore size cellulose acetate filter (Sartorius, Göttingen, Germany) and stored at 4°C until
284 analysis. Ammonium was measured with ion chromatography (Metrohm, Herisau, Switzerland) and
285 nitrate with a flow-injection analyzer (SAN++, Skalar, Breda, The Netherlands). A total organic carbon
286 analyzer (Shimadzu, Kyoto, Japan) was used for DIC quantification. Water samples for flow cytometry
287 were fixed with formaldehyde and stained with SYBR Green I (Thermo Fisher Scientific, Waltham, MA,
288 USA) at 37°C for 15 min. Particles were counted on an Accuri C6 flow cytometer (BD Biosciences, San
289 Jose, CA, USA) and microbial cell counts determined as described previously (Proctor et al. 2018).

290 Samples for methane measurements were injected into airtight 40 ml serum vials filled with N_2 gas
291 and 4 g NaOH pellets (≥98% purity, Sigma-Aldrich, Darmstadt, Germany) for preservation. Gas
292 chromatography (6890N, Agilent Technologies, Santa Clara, CA, USA) was used to measure methane
293 in the headspace. The GC was equipped with a Carboxen 1010 column (Supelco, Bellefonte, PA, USA)
294 and a flame ionization detector. Control experiments showed that 4 g of solid NaOH produced 32.6
295 nmol CH_4 on average which was accounted for when back-calculating methane concentrations in
296 water based on Wiesenburg and Guinasso (1979).

297 ## Nucleic acid purification

298 110 ml lake water were filtered on site through 0.2 µm cellulose acetate filters (Sartorius) and instantly
299 frozen on dry ice and stored at -80 °C in the laboratory until extraction. Genomic DNA and total RNA
300 were extracted with the AllPrep DNA/RNA Mini Kit (Qiagen, Hilden, Germany) with a bead beating
301 step on a FAstPrep-24 (MP Biomedicals, Santa Ana, CA, USA) and 150-212 µm glass beads. Residual
302 DNA in RNA extracts was digested using the TURBO DNA-free kit (Thermo Fisher Scientific). DNA
303 removal was checked by gel electrophoresis after PCR (16S rRNA gene, 27f/1492r, 35 cycles) and if
304 required a second digestion was performed. cDNA was reverse transcribed from RNA with random
305 hexamers using SuperScript IV First-Strand Synthesis System (Thermo Fisher Scientific). DNA and cDNA
306 were used for Illumina MiSeq sequencing and qPCR.

307 ## 16S rRNA and *pmoA* sequencing and analysis

308 Bacterial 16S rRNA gene and rRNA (S-D-Bact-0341-b-S-17, D-Bact-0785-a-A-21) (Klindworth et al.
309 2013) and functional marker *pmoA* gene and transcript (189f, mb661) (Costello and Lidstrom 1999)
310 amplicon libraries were sequenced on the Illumina MiSeq platform (Illumina Inc., San Diego, CA, USA).
311 Briefly, the first PCR was performed in triplicate with tailed forward and reverse primers using
312 NEBNext Q5® Hot Start HiFi PCR Master Mix (New England BioLabs, Hitchin, UK) and 17 and 25 cycles
313 for the bacterial and functional marker, respectively. To pooled and purified products Illumina

314 barcodes and adapters were attached in a second PCR (8 cycles) with the Nextera XT Index Kit A and
315 D (Illumina Inc.). Libraries were purified with Agencourt AMPure XP kit (Beckman coulter, Indianapolis,
316 IN, USA), quantified (Qubit, Thermo Fischer Scientific) and pooled. After quality check on a Tape
317 Station 2200 (Agilent Genomics, USA) the two sequencing runs with 600-cycle MiSeq reagent kit v3
318 and 10% PhiX were performed at the Genetic Diversity Centre (ETH Zurich).

319 Amplicon sequence variants (ASVs) were inferred with the DADA2 pipeline (Callahan et al. 2016)
320 (v1.6.0) in R (R Core Team 2017) (v3.4.1). Reads reaching a quality score of two were truncated and
321 reads with ambiguous bases or an expected error rate exceeding three were removed. 16S rRNA reads
322 were trimmed to 270 nt (forward) and 210 nt (reverse) and *pmoA* reverse reads were trimmed to 235
323 nt. The ASV table was produced following the DADA2 pipeline. Taxonomy of 16S rRNA ASVs was
324 assigned using the SILVA reference database (v132) (Quast et al. 2013) and reads assigned to
325 mitochondria or chloroplasts were removed with phyloseq (McMurdie and Holmes 2013) (1.24.2) in
326 R (3.5.0). The 16S rRNA data set was screened for known methanotrophic groups (Knief 2015) within
327 the order *Methylococcales*, genera within class *Alphaproteobacteria* and phylum *Verrucomicrobia*,
328 and *Candidatus* Methylomirabilis. ASVs reaching >0.2% relative abundance in at least 3 samples were
329 retained for further analysis. Amino acid sequences (aaASV) were derived from *pmoA* ASVs in MEGA7
330 and were retained for further analyses (Kumar et al. 2016) when exceeding 2% relative abundance in
331 at least one sample. Neighbor-joining trees were constructed in MEGA7 with 10000 bootstrap
332 replications using Jukes-Cantor evolutionary distance for 16S rRNA sequences or Poisson correction
333 method for *pmoA* amino acid sequences. To facilitate interpretation we assigned the same colors for
334 MOB ASVs (MOB-affiliated 16S rRNA amplicon sequence variants) and aaASVs (*pmoA* amino acid
335 operational taxonomic units) if they (i) showed similar relative abundance and distribution pattern as
336 observed in a canonical correspondence analysis (Supplementary Fig. 2), and (ii) placement in the
337 phylogenetic trees was compatible with this interpretation. To quantify MOB dynamics in terms of cell
338 numbers we applied CARD-FISH. To track the activity of present MOB we measured potential methane

339 oxidation rates in incubations with $^{13}C\text{-}CH_4$. All measures of MOB abundance and activity were
340 significantly and positively correlated (Tab. 1).

341 ## *pmoA* gene and transcript quantification

342 The amount of *pmoA* DNA and mRNA copies in lake water during overturn was quantified by qPCR
343 using the 189f-mb661 primer pair (Costello and Lidstrom 1999) on a LightCycler 480 (Roche
344 Diagnostics, Rotkreuz, Switzerland). 10µl reactions were performed with 0.2 µM primer, 2 µl of 1:10
345 diluted DNA or cDNA and the SYBR Green I Master mix (Roche). We used PCR conditions adapted from
346 Henneberger et al. 2015 (Henneberger et al. 2015) with 10 min initial denaturation, 15 s denaturation
347 during cycling and acquisition at 79°C. Standards were obtained by 10-fold dilutions of *pmoA*
348 containing plasmid, which were measured in quadruplicates. Sample assays were performed in
349 triplicates and analysed with the LightCycler 480 software (v1.5.1.62) with the second derivative
350 maximum method.

351 ## Potential methane oxidation rates

352 Water samples were filled into 60 ml serum vials in the field and incubations started the same day
353 upon arrival in the laboratory. The applied procedure to determine potential methane oxidation was
354 adapted from Oswald et al. 2015 (Oswald et al. 2015). Each sample was purged with N_2 to remove
355 residual methane, amended with non-limiting concentrations of oxygen (~50 µmol L^{-1}) and $^{13}C\text{-}CH_4$
356 (~80 µmol L^{-1}), and subdivided into five Exetainers (Holtappels et al. 2011) (6ml) that were kept dark
357 and close to the *in-situ* temperature of the mixed layer as determined at the date of sampling.
358 Incubations were stopped after 0, 3, 13, 25 and 50 hours with 100 µl $ZnCl_2$ 50% w/v. The increase of
359 $^{13}C\text{-}CO_2$ was determined with GC-IRMS (IsoPrime, Micromass, Wilmslow, UK). Rates were derived from
360 a linear regression of the $^{13}C\text{-}CO_2$ production over time, taking into account the background DIC in the
361 sample. Carrara marble (ETH Zurich, $\delta^{13}C$ of 2.1‰) served as a standard.

362 ## MOB quantification with CARD-FISH

363 Samples were fixed with formaldehyde (2% final concentration) for 3-6 hours on ice prior to filtration
364 onto 0.2 µm polycarbonate nuclepore track-etched membrane filters (Whatman, Maidstone, UK). Dry
365 filters were stored at -20°C until further processing. Filters were embedded in 0.2% low gelling point
366 agarose (Metaphor, Lonza), cells were permeabilized with lysozyme (10 mg ml^{-1}) for 70 min at 37°C
367 and peroxidases inactivated in 10 mM HCl for 10 min. The probes Mg84, Mg669 and Mg705 (Eller et
368 al. 2001) were mixed to target type I MOB. As control probes EUB338I-III (universal bacterial probe,
369 positive control) and NON338 (negative control) (Wallner et al. 1993, Daims et al. 1999) were
370 separately applied to each sample. Filters were incubated at 46°C for 2.5 h with 150 µl of the
371 respective hybridization buffer (20% formamide Mg-mix and 35% for EUB and NON) containing 1 µl of
372 probe (50 ng $µl^{-1}$). After washing, filters were placed into the amplification buffer containing Oregon
373 Green 488 at 37°C for 30 min in the dark. DAPI was used for counterstaining and the filters were
374 mounted on glass slides in a mix of Citifluor and Vectashield (4:1).

375 Epifluorescence images were taken with an inverted microscope (DMI6000 B, Leica, Wetzlar,
376 Germany) and a 100x/1.3 objective (PL-FL, Leica). To obtain clear images multifocual images were
377 recorded and merged with LASX software (Leica). DAPI and the corresponding CARD-FISH images of
378 22 randomly selected fields per filter were used for semi-automated cell counting with daime (Daims
379 et al. 2006) software. In daime, image histograms were adjusted manually, objects were detected with
380 the edge detection algorithm and split with a watershed segmentation-based algorithm. Object
381 detection was improved manually if necessary. Median of cell numbers multiplied by the mixed layer
382 volume were used to calculate growth rates (r) using the natural logarithm plotted against time (Oct
383 – Dec 12). Doubling times were derived as $dt = \ln(2)/r$ (Graham et al. 2009).

Statistics

Canonical correspondence analysis (CCA) was performed on the MOB ASV relative abundance among bacterial 16S rRNA gene sequences and the aaASV percentage of *pmoA* mRNA sequences using scaled physicochemical parameters (O_2 and CH_4 concentrations and temperature) with phyloseq (McMurdie and Holmes 2013) in R. Constrained axes were tested for significance with anova.cca of vegan v2.5.2. The methane oxidation capacity was calculated based on the median potential methane oxidation rate in the mixed layer multiplied by the volume of the mixed layer.

Data availability

The sequencing files have been submitted to the European nucleotide archive under the project number PRJEB32413.

Acknowledgements

We thank Carsten Schubert and Serge Robert for access to the GC-IRMS and support with methane oxidation rate measurements. We further thank Karin Beck, Patrick Kathriner, Miro Meyer and Michael Plüss for assistance in the field and laboratory. We thank Carsten Schubert and Bernhard Wehrli for their support and helpful discussions. Sequencing data generation and analysis was done in collaboration with the Genetic Diversity Centre (GDC), ETH Zurich. The research was funded by Swiss National Science Foundation (grant CR23I3_156759).

References

Bastviken, D., J. J. Cole, M. L. Pace, and M. C. Van de-Bogert. 2008. Fates of methane from different lake habitats: Connecting whole-lake budgets and CH4 emissions. Journal of Geophysical Research: Biogeosciences 113:1–13.

Bastviken, D., J. Cole, M. Pace, and L. Tranvik. 2004. Methane emissions from lakes: Dependence of lake characteristics, two regional assessments, and a global estimate. Global Biogeochemical Cycles 18:1–12.

Bastviken, D., J. Ejlertsson, and L. Tranvik. 2002. Measurement of methane oxidation in lakes: A comparison of methods. Environmental Science and Technology 36:3354–3361.

Beaulieu, J. J., T. DelSontro, and J. A. Downing. 2019. Eutrophication will increase methane emissions from lakes and impoundments during the 21st century. Nature Communications 10:1375.

Benjamini, Y., and Y. Hochberg. 1995. Controlling the false discovery rate: a practical and powerful approach to multiple testing. Journal of the Royal Statistical Society B 57:289–300.

Biderre-Petit, C., D. Jézéquel, E. Dugat-Bony, F. Lopes, J. Kuever, G. Borrel, E. Viollier, G. Fonty, and P. Peyret. 2011. Identification of microbial communities involved in the methane cycle of a freshwater meromictic lake. FEMS Microbiology Ecology 77:533–545.

Blees, J., H. Niemann, C. B. Wenk, J. Zopfi, C. J. Schubert, M. K. Kirf, M. L. Veronesi, C. Hitz, and M. F. Lehmann. 2014. Micro-aerobic bacterial methane oxidation in the chemocline and anoxic water column of deep south-Alpine Lake Lugano (Switzerland). Limnology and Oceanography 59:311–324.

Callahan, B. J., P. J. Mcmurdie, M. J. Rosen, A. W. Han, A. J. Johnson, and S. P. Holmes. 2016. DADA2 : High resolution sample inference from amplicon data. Nature Methods 13:581–583.

423 Costello, A. M., and M. E. Lidstrom. 1999. Molecular characterization of functional and phylogenetic
424 genes from natural populations of methanotrophs in lake sediments. Applied and
425 environmental microbiology 65:5066–74.

426 Daims, H., A. Brühl, R. Amann, K. H. Schleifer, and M. Wagner. 1999. The domain-specific probe
427 EUB338 is insufficient for the detection of all bacteria: Development and evaluation of a more
428 comprehensive probe set. Systematic and Applied Microbiology 22:434–444.

429 Daims, H., S. Lücker, and M. Wagner. 2006. Daime, a Novel Image Analysis Program for Microbial
430 Ecology and Biofilm Research. Environmental Microbiology 8:200–213.

431 DelSontro, T., J. J. Beaulieu, and J. A. Downing. 2018. Greenhouse gas emissions from lakes and
432 impoundments: Upscaling in the face of global change. Limnology and Oceanography Letters
433 3:64–75.

434 Eller, G., S. Stubner, and P. Frenzel. 2001. Group-specific 16S rRNA targeted probes for the detection
435 of type I and type II methanotrophs by fluorescence in situ hybridisation. FEMS Microbiology
436 Letters 198:91–97.

437 Encinas Fernández, J., F. Peeters, and H. Hofmann. 2014. Importance of the autumn overturn and
438 anoxic conditions in the hypolimnion for the annual methane emissions from a temperate lake.
439 Environmental Science and Technology 48:7297–7304.

440 Graham, L. E., J. M. Graham, and L. W. Wilcox. 2009. Algae. 2nd ed. Pearson Benjamin Cummings,
441 San Francisco.

442 Henneberger, R., E. Chiri, P. L. E. Bodelier, P. Frenzel, C. Lüke, and M. H. Schroth. 2015. Field-scale
443 tracking of active methane-oxidizing communities in a landfill cover soil reveals spatial and
444 seasonal variability. Environmental Microbiology 17:1721–1737.

445 Holtappels, M., G. Lavik, M. M. Jensen, and M. M. M. Kuypers. 2011. 15N-labeling experiments to
446 dissect the contributions of heterotrophic denitrification and anammox to nitrogen removal in
447 the OMZ waters of the ocean. Methods in Enzymology 486:224–246.

448 Jenny, J.-P., A. Normandeau, P. Francus, Z. E. Taranu, I. Gregory-Eaves, F. Lapointe, J. Jautzy, A. E. K.
449 Ojala, J.-M. Dorioz, A. Schimmelmann, and B. Zolitschka. 2016. Urban point sources of nutrients
450 were the leading cause for the historical spread of hypoxia across European lakes. Proceedings
451 of the National Academy of Sciences 113:12655–12660.

452 Kankaala, P., S. Taipale, H. Nykänen, and R. I. Jones. 2007. Oxidation, efflux, and isotopic
453 fractionation of methane during autumnal turnover in a polyhumic, boreal lake. Journal of
454 Geophysical Research: Biogeosciences 112:1–7.

455 Kirf, M. K., C. Dinkel, C. J. Schubert, and B. Wehrli. 2014. Submicromolar oxygen profiles at the oxic-
456 anoxic boundary of temperate lakes. Aquatic Geochemistry 20:39–57.

457 Kirf, M. K., H. Røy, M. Holtappels, J. P. Fischer, C. J. Schubert, and B. Wehrli. 2015. Redox gradients at
458 the low oxygen boundary of lakes. Aquatic Sciences 77:81–93.

459 Klindworth, A., E. Pruesse, T. Schweer, J. Peplies, C. Quast, M. Horn, and F.-O. Glöckner. 2013.
460 Evaluation of general 16S ribosomal RNA gene PCR primers for classical and next-generation
461 sequencing-based diversity studies. Nucleic Acids Research 41:1–11.

462 Knief, C. 2015. Diversity and habitat preferences of cultivated and uncultivated aerobic
463 methanotrophic bacteria evaluated based on pmoA as molecular marker. Frontiers in
464 Microbiology 6:1–38.

465 Kojima, H., T. Iwata, and M. Fukui. 2009. DNA-based analysis of planktonic methanotrophs in a
466 stratified lake. Freshwater Biology 54:1501–1509.

467 Kumar, S., G. Stecher, and K. Tamura. 2016. MEGA7: Molecular evolutionary genetics analysis
468 version 7.0 for bigger datasets. Molecular biology and evolution 33:1870–1874.

469 McMurdie, P. J., and S. Holmes. 2013. Phyloseq: An R Package for Reproducible Interactive Analysis
470 and Graphics of Microbiome Census Data. PLoS ONE 8:1–11.

471 Messager, M. L., B. Lehner, G. Grill, I. Nedeva, and O. Schmitt. 2016. Estimating the volume and age
472 of water stored in global lakes using a geo-statistical approach. Nature Communications 7:1–
473 11.

474 Myhre, G., D. Shindell, F.-M. Bréon, W. Collins, J. Fuglestvedt, J. Huang, D. Koch, J.-F. Lamarque, D.
475 Lee, B. Mendoza, T. Nakajima, A. Robock, G. Stephens, T. Takemura, and H. Zhang. 2013.
476 Anthropogenic and natural radiative forcing. Pages 659–740 *in* P. M. M. Stocker, T.F., D. Qin,
477 G.-K. Plattner, M. Tignor, S.K. Allen, J. Boschung, A. Nauels, Y. Xia, V. Bex, editor. Climate
478 Change 2013: The Physical Science Basis. Contribution of Working Group I to the Fifth
479 Assessment Report of the Intergovernmental Panel on Climate Change. Cambridge University
480 Press, Cambridge, UK and New York, NY, USA.

481 Oswald, K., J. S. Graf, S. Littmann, D. Tienken, A. Brand, B. Wehrli, M. Albertsen, H. Daims, M.
482 Wagner, M. M. M. Kuypers, C. J. Schubert, and J. Milucka. 2017. Crenothrix are major methane
483 consumers in stratified lakes. ISME Journal 11:2124–2140.

484 Oswald, K., J. Milucka, A. Brand, S. Littmann, B. Wehrli, M. M. M. Kuypers, and C. J. Schubert. 2015.
485 Light-dependent aerobic methane oxidation reduces methane emissions from seasonally
486 stratified lakes. PLoS ONE 10:1–22.

487 Proctor, C. R., M. D. Besmer, T. Langenegger, K. Beck, J. C. Walser, M. Ackermann, H. Bürgmann, and
488 F. Hammes. 2018. Phylogenetic clustering of small low nucleic acid-content bacteria across
489 diverse freshwater ecosystems. ISME Journal 12:1344–1359.

Quast, C., E. Pruesse, P. Yilmaz, J. Gerken, T. Schweer, P. Yarza, J. Peplies, and F.-O. Glöckner. 2013. The SILVA ribosomal RNA gene database project: Improved data processing and web-based tools. Nucleic Acids Research 41:590–596.

R Core Team. 2017. A language and environment for statistical computing. Vienna, Austria.

Rahalkar, M., I. Bussmann, and B. Schink. 2007. Methylosoma difficile gen. nov., sp. nov., a novel methanotroph enriched by gradient cultivation from littoral sediment of Lake Constance. International Journal of Systematic and Evolutionary Microbiology 57:1073–1080.

Salcher, M. M. 2014. Same same but different: ecological niche partitioning of planktonic freshwater prokaryotes. Journal of Limnology 73:74–87.

Schubert, C. J., T. Diem, and W. Eugster. 2012. Methane emissions from a small wind shielded lake determined by eddy covariance, flux chambers, anchored funnels, and boundary model calculations: A comparison. Environmental Science and Technology 46:4515–4522.

Schubert, C. J., F. S. Lucas, E. Durisch-Kaiser, R. Stierli, T. Diem, O. Scheidegger, F. Vazquez, and B. Müller. 2010. Oxidation and emission of methane in a monomictic lake (Rotsee, Switzerland). Aquatic Sciences 72:455–466.

Taipale, S., P. Kankaala, M. Hahn, R. Jones, and M. Tiirola. 2011. Methane-oxidizing and photoautotrophic bacteria are major producers in a humic lake with a large anoxic hypolimnion. Aquatic Microbial Ecology 64:81–95.

Trotsenko, Y. A., and V. N. Khmelenina. 2005. Aerobic methanotrophic bacteria of cold ecosystems. FEMS Microbiology Ecology 53:15–26.

Utsumi, M., Y. Nojiri, T. Nakamura, T. Nozawa, A. Otsuki, N. Takamura, M. Watanabe, and H. Seki. 1998. Dynamics of dissolved methane and methane oxidation in dimitic Lak Nojiri during

512 winter. Limnology and Oceanography 43:10–17.

513 Wallner, G., R. Amann, and W. Beisker. 1993. Optimizing fluorescent in sit hybridization with rRNA-
514 targeted oligonucleotide probes for flow cytometric identification of microorganisms.
515 Cytometry 14:136–143.

516 Wiesenburg, D. A., and N. L. Guinasso. 1979. Equilibrium solubilities of methane, carbon monoxide,
517 and hydrogen in water and sea water. Journal of Chemical and Engineering Data 24:356–360.

518 Wise, M. G., J. V McArthur, and L. J. Shimkets. 2001. Methylosarcina fibrata gen. nov., sp. nov. and
519 Methylosarcina quisquiliarum sp.nov., novel type 1 methanotrophs. International Journal of
520 Systematic and Evolutionary Microbiology 51:611–621.

521 Zimmermann, M., M. J. Mayr, D. Bouffard, W. Eugster, T. Steinsberger, B. Wehrli, A. Brand, and H.
522 Bürgmann. 2019. Lake overturn as a key driver for methane oxidation. bioRxiv.

523